INTERNATIONAL JOURNAL FOR NUMERICAL METHODS IN FLUIDS
Int. J. Numer. Meth. Fluids 2000; **33**: 711–736

Compact high-resolution algorithms for time-dependent advection on unstructured grids

M. E. Hubbard[a,*,1] and P. L. Roe[b,c]

[a] *The University of Reading, Department of Mathematics, Whiteknights, Reading, U.K.*
[b] *Department of Aerospace Engineering, University of Michigan, Ann Arbor, MI, U.S.A.*
[c] *Centre pour Mathematiques et leurs Applications, Ecole Normale Superieure de Cachan, 61 Avenue du President Wilson, Cachan Cedex, France*

SUMMARY

A technique for constructing monotone, high resolution, multi-dimensional upwind fluctuation distribution schemes for the scalar advection equation is presented. The method combines the second-order Lax–Wendroff scheme with the upwind positive streamwise invariant (PSI) scheme via a fluctuation redistribution step, which ensures monotonicity (and which is a generalization of the flux-corrected transport approach for fluctuation distribution schemes). Furthermore, the concept of a distribution point is introduced, which, when related to the equivalent equation for the scheme, leads to a 'preferred direction' for the limiting procedure, and hence to a new distribution of the fluctuation, which retains second-order accuracy from the Lax–Wendroff scheme, even when the solution contains turning points. Experimental comparisons show that the new method compares favourably in terms of speed, accuracy and robustness with other, similar, techniques. Copyright © 2000 John Wiley & Sons, Ltd.

KEY WORDS: high resolution; limiters; monotonic; multi-dimensional upwinding; scalar advection equation; time-dependent

1. INTRODUCTION

Over the last 10 years a family of cell vertex finite volume methods (FVM) for the solution of the two-dimensional scalar advection equation has evolved, collectively known as multi-dimensional upwind fluctuation distribution schemes (or some variant thereon), see, for example, References [1–8], the last two of which cite many additional references. For the approximation of steady state flows on unstructured triangular grids, these have reached a degree of maturity whereby the multi-dimensional schemes reproduce most of the advantages of upwind schemes in one dimension: second-order approximation of smooth solutions, monotonicity in the

* Correspondence to: The University of Reading, Department of Mathematics, P.O. Box 220, Whiteknights, Reading RG6 6AX, U.K. Tel.: +44 118 9875123, ext. 4009; fax: +44 0118 9313423.
[1] E-mail: m.e.hubbard@reading.ac.uk

Received November 1998
Revised May 1999

presence of discontinuities and rapid convergence to the steady state without the necessity for additional artificial viscosity. A distinctive and attractive feature of these schemes is that they are computationally compact. They can be written as loops over elements, and when processing an element, no reference is made to data outside that element. This makes for efficient parallelization. A theoretical attraction is that the update scheme can incorporate insights derived from the nature of the multi-dimensional physics [9]. Practical application of the method has been reported by Khobalatte and Leyland [10] and by Stoufflet [private communication].

Unfortunately, most of the upwind distribution schemes developed for steady state problems are only first-order accurate for time-dependent flows. This short-coming has been addressed with some success in Reference [3] in which the schemes have been equated with upwind finite element algorithms, but only at the expense of inverting a full mass matrix. Further, this method allow spurious oscillations to occur in the solution close to steep gradients, so a flux-corrected transport step is applied [2,11,12] to ensure monotonicity. A predictor–corrector method [2] in the style of MacCormack's one-dimensional scheme [13] has also been constructed, but this has only proved to be successful in a limited range of situations.

In this paper an alternative approach to the creation of monotone high-resolution fluctuation distribution schemes will be described. Two explicit fluctuation distribution schemes [1], the monotone positive streamwise invariant (PSI) scheme and the second-order accurate Lax–Wendroff scheme, are combined in the style of flux-corrected transport but in a manner that provides greater flexibility. The limiting procedure that enforces monotonicity is written as a fluctuation redistribution step in which the distribution coefficients of the underlying scheme are altered in such a way that the discretization satisfies a local maximum principle, while retaining conservation and as much of the accuracy of the basic high-order scheme as possible.

For triangular elements, redistribution of the fluctuation involves three degrees of freedom in each element, reduced to two by enforcing conservation. A slope limiting procedure, such as the monotone upstream-centred scheme for conservation laws (MUSCL) [14], also has two degrees of freedom, sometimes reduced to one by requiring that the direction of the gradient vector is not changed. The unique feature of the present method is that the two degrees of freedom are co-ordinated whenever possible to retain, in a certain sense, local second-order accuracy. To achieve this, the concept of a distribution point for a fluctuation distribution scheme will be described and related to monotonicity conditions derived from the local solution. These conditions define a region in which the distribution point should lie. Furthermore, the equivalent equation for the scheme will be used to construct a preferred direction for the movement of the distribution point when the redistribution is carried out.

In Section 2 current multi-dimensional upwind schemes for solving steady state problems are described. Section 3 describes the technique of fluctuation redistribution, which is used to impose monotonicity and methods by which high-order accuracy can be retained. Result are presented for two time-dependent scalar advection test cases in Section 4, followed by a brief disussion of conclusions and further work in Section 5.

2. STEADY STATE SCHEMES

Consider the two-dimensional scalar advection equation

$$u_t + f_x + g_y = 0 \quad \text{or} \quad u_t + \vec{\lambda}\cdot\vec{\nabla}u = 0 \tag{2.1}$$

where

$$\vec{\lambda} = \left(\frac{\partial f}{\partial u}, \frac{\partial g}{\partial u}\right)^T$$

defines the advection velocity. The fluctuation associated with this equation is a cell-based quantity that, in the case of a divergence-free advection velocity $\vec{\nabla}\cdot\vec{\lambda} = 0$, is given by

$$\phi = -\iint_{\triangle} \vec{\lambda}\cdot\vec{\nabla}u \, \mathrm{d}x \, \mathrm{d}y = \oint_{\partial\triangle} u\vec{\lambda}\cdot\mathrm{d}\vec{n} \tag{2.2}$$

where $\vec{n}$ represents the inward pointing normal to the boundary of the cell.

The numerical scheme is constructed from a discretization of the integrated form of Equation (2.1) by evaluating the quantity ϕ, defined in Equation (2.2), within each cell and then distributing it to the nodes of the grid, i.e. a distribution of the fluctuation carried out.

The discrete form of ϕ is evaluated using an appropriate (conservative) linearization [1]. When the integration in Equation (2.2) can be carried out exactly, the fluctuation can be written

$$\phi = -S_{\triangle}\hat{\vec{\lambda}}\cdot\vec{\nabla}u \tag{2.3}$$

where $S_{\triangle}$ is the cell area and the symbol $\hat{\cdot}$ indicates an appropriately linearized quantity. In the special case of linear advection, a conservation linearization can be constructed simply by assuming that u varies linearly over each triangle with the discrete solution values stored at the nodes and continuity across the edges of the mesh cells [1].

Combining the above approximation of the flux terms with a simple forward Euler discretization of the time derivative leads to an iterative update of the nodal solution values, which is generally written [1] as

$$u_i^{n+1} = u_i^n + \frac{\Delta t}{S_i}\sum_{j\in\cup\triangle_i} \alpha_i^j \phi_j \tag{2.4}$$

where S_i is the area of the median dual cell corresponding to node i (one third of the total area of the triangles with a vertex at i), α_i^j is the distribution coefficient, which indicates the appropriate proportion of the fluctuation ϕ_j, to be sent from cell j to node i, and $\cup\triangle_i$ represents the set of cells with vertices at node i. Conservation is assured as long as

$$\sum_{i \in \triangle_j} \alpha_i^j = 1, \quad \forall j \tag{2.5}$$

where $\triangle_j$ represents here the set of nodes at the vertices of cells j, i.e. the whole of each fluctuation is sent to the nodes.

In fact, the accuracy of these schemes can be improved slightly by altering the weighting of the nodal updates in a manner that ensures that linear initial data on an arbitrary grid remains linear after each time step [Barth TJ. Private communication; 2]. This is equivalent to constructing a consistent, mass-lumped upwind discretization of the equation. The resulting nodal update, given by

$$u_i^{n+1} = u_i^n + \frac{\Delta t}{\sum_{j \in \cup \triangle_i} \alpha_i^j S_{\triangle_j}} \sum_{j \in \cup \triangle_i} \alpha_i^j \phi_j \tag{2.6}$$

has been used in all PSI scheme computations reported here. This replaces the fixed area S_i associated with the ith node by $\Sigma\, \alpha_j^i S_{\triangle_j}$ wherever S_i appears. Note that this modification has no effect on the conservative nature of the distribution scheme.

2.1. The PSI scheme

The distribution coefficients for the PSI scheme, α_i^j in (2.4), chosen so that the resulting scheme is conservative, linearity preserving (second-order accurate at the steady state) and positive (monotone). There is generally some degree of ambiguity associated with the definition of 'monotone' in two dimensions, but here it will always be used to denote a scheme that does not create new extrema at the next time level.

The PSI scheme, which was devised by Struijs [6] and formulated algebraically by Sidilkover and Roe [5] as follows, has all of the above properties.

1. For each triangle, locate the downstream vertices, i.e. those for which

$$\vec{\lambda} \cdot \vec{n}_i > 0 \tag{2.7}$$

   where $\vec{n}_i$ is the inward pointing normal to the edge opposite vertex i.
2. If a triangle has a single downstream vertex, node i say, then that node receives the whole fluctuation, so

$$u_i \rightarrow u_i + \frac{\Delta t}{S_i} \phi \tag{2.8}$$

   while the values of u at the other two vertices remain unchanged.
3. Otherwise the triangle has two downstream vertices, i and j say, and the fluctuation is divided between these two nodes so that

$$u_i \to u_i + \frac{\Delta t}{S_i}\phi_i^*, \qquad u_j \to u_j + \frac{\Delta t}{S_j}\phi_j^* \tag{2.9}$$

where $\phi_i^* + \phi_j^* = \phi$.
The fluctuations in Equation (2.9) are defined as the limited quantities

$$\phi_i^* = \phi_i - L(\phi_i, -\phi_j), \qquad \phi_j^* = \phi_j - L(\phi_j, -\phi_i) \tag{2.10}$$

where

$$\phi_i = -\frac{1}{2}\vec{\lambda}\cdot\vec{n}_i(u_i - u_k), \qquad \phi_j = -\frac{1}{2}\vec{\lambda}\cdot\vec{n}_j(u_j - u_k) \tag{2.11}$$

in which k denotes the remaining (upstream) vertex of the triangle and L denotes the minmod limiter function

$$L(x, y) = \frac{1}{2}(1 + \mathrm{sgn}(xy))\frac{1}{2}(\mathrm{sgn}(x) + \mathrm{sgn}(y))\min(|x|, |y|) \tag{2.12}$$

The scheme is globally positive and therefore stable, the appropriate restriction on the time step being

$$\Delta t \le \frac{S_i}{\sum_{j \in \cup \triangle_i} \max\left(0, \frac{1}{2}\vec{\lambda}_j\cdot\vec{n}_i^j\right)} \tag{2.13}$$

The above algorithm is second-order accurate only at the steady state. This can be explained by considering the application of the limiter in step (3). It takes the contributions ϕ_i and ϕ_j (2.11) due to the first-order N scheme [1] and redistributes the fluctuation between the two downstream vertices (along the outflow edge), which, in some sense, gives second-order accuracy only in the cross-stream direction. The scheme is first-order accurate in the streamwise direction (in fact, on a regular grid with edges aligned with the flow, it reduces to the one-dimensional first-order upwind scheme), however, at the steady state this is irrelevant because the solution is constant parallel to the streamlines.

In the following sections, the PSI scheme will be used as the basis of a monotone second-order accurate scheme for approximating time varying solutions of the two-dimensional scalar advection equation on triangular grids.

2.2. The Lax–Wendroff distribution scheme

The Lax–Wendroff scheme [1] is the unique single-step, second-order accurate fluctuation distribution scheme on triangles with a compact stencil (each nodal update depends only on the solution values at neighbouring nodes). The distribution coefficients required by Equation (2.4) to give this scheme are

$$\alpha_i^j = \frac{1}{3} + \frac{\Delta t}{4S_{\triangle_j}} \vec{\lambda}_j \cdot \vec{n}_i^j \tag{2.14}$$

where $S_{\triangle_j}$ is the area of the jth cell and $\vec{n}_i^j$ is the scaled inward pointing normal to the edge of triangle j opposite the vertex at node i. The limit on the time step at a node i for the stability of this scheme is taken to be

$$\Delta t \leq 2 \min_{j \in \cup \triangle_i} \left(\frac{S_{\triangle_j}}{\max_{l \in \triangle_j} |\vec{\lambda}_j \cdot \vec{n}_l^j|} \right) \tag{2.15}$$

where the index l cover the vertices of each cell in the local patch surrounding the node.

3. LIMITING BY FLUCTUATION REDISTRIBUTION

The new fluctuation redistribution technique combines two numerical schemes, a low-order monotone scheme, taken here to be the PSI scheme of Section 2, and a high-order (non-monotone) scheme to which the smoothing will be applied, such as the Lax–Wendroff scheme. The technique can be considered as a generalization of the flux-corrected transport (FCT) algorithm [12,15] and as such requires that each of the underlying schemes be written in a form that isolates the contribution of each individual grid cell to the nodes of the grid. An anti-diffusive cell contribution is then calculated by taking the difference between the high-order and low-order contributions. This is then limited in such a way as to prohibit unwanted extrema in the solution while retaining as much of the anti-diffusive component as possible. As a result, the high-order scheme should dominate the algorithm in smooth regions of the flow while the first-order scheme is favoured where the solution gradient is locally high.

The fluctuation redistribution algorithm can be described in the notation of Reference [12] by the following simple steps:

1. For each element
   (a) Compute the low-order element contribution (LEC) from the PSI scheme.
   (b) Compute the high-order element contribution (HEC) from the Lax–Wendroff scheme.
   (c) Calculate the anti-diffusive element contribution (AEC), as given by

$$\text{AEC} = \text{HEC} - \text{LEC} \tag{3.1}$$

2. For each node
   - Compute the updated low-order solution

$$u_i^{\text{L}} = u_i^n + \sum_{j \in \cup \triangle_i} \text{LEC}_i^j \tag{3.2}$$

3. For each element
   - Correct the AEC to each cell vertex so that conservation is retained and the new solution (as defined in step (4)) has no extrema not also found in either u_i^{L} or u_i^n, so

$$\mathrm{AEC}_i^j \to \beta_i^j \times \mathrm{AEC}_i^j \tag{3.3}$$

where, usually, $0 \le \beta_i^j \le 1$. The crucial ingredient here is the computation of β_i^j, which is discussed in detail below.

Note that the FCT approach consists of using a single β for each triangle, i.e. $\beta_i^j = \beta^j$, which automatically ensures conservation. In the present formulation, the possibility of using a different β for each node is considered. Care must be taken to ensure conservation, which is achieved as long as the final scheme can be cast as a distribution scheme (2.4) satisfying the conservation condition (2.5). The distribution point concept introduced in the next section is particularly useful in this respect.

4. For each node
   - Calculate the final solution update

$$u_i^{n+1} = u_i^{\mathrm{L}} + \sum_{j \in \cup \triangle_i} \mathrm{AEC}_i^j \tag{3.4}$$

The limiting procedure of step (3) is designed to make AEC_i^j as large as possible without introducing new extrema and without knowing in advance the nodal updates due to the high-order scheme in adjacent cells. It involves the following calculations within each triangular element:

(i) Evaluate, in order, the quantities

$$u_i^* = \begin{Bmatrix} \max \\ \min \end{Bmatrix} (u_i^{\mathrm{L}}, u_i^n)$$

$$u_j^* = \begin{Bmatrix} \max \\ \min \end{Bmatrix} u_i^*, \quad \forall i \in \triangle_j \tag{3.5}$$

$$u_i^{\begin{smallmatrix} \max \\ \min \end{smallmatrix}} = \begin{Bmatrix} \max \\ \min \end{Bmatrix} u_j^*, \quad \forall j \in \cup \triangle_i$$

the last of which give the extreme values of the solution at each node i, beyond which the updated solution is not allowed to go. Note that u_i^{L} can be calculated for this purpose using the maximum stable local time step (rather than the actual time step) to give the least restrictive bounds on the nodal updates.

(ii) Define

$$P_i^{\pm} = \sum_{j \in \cup \triangle_i} \begin{matrix} \max \\ \min \end{matrix} (0, \mathrm{AEC}_i^j)$$

$$Q_i^{\pm} = u_i^{\max\atop\min} - u_i^{\mathrm{L}} \tag{3.6}$$

and subsequently

$$W_i^{\pm} = \begin{cases} \min(1,\ Q_i^{\pm}/P_i^{\pm}) & \text{if } P_i^{+} > 0,\ P_i^{-} < 0 \\ 0 & \text{if } P_i^{\pm} = 0 \end{cases} \tag{3.7}$$

a nodal limiting factor for the anti-diffusive contribution, which ensures that the new solution value at node i does not violate the prescribed bounds.

(iii) Finally, calculate

$$(\beta_i^j)^{\max} = \begin{cases} W_i^{+} & \text{if } \mathrm{AEC}_i^j \geq 0 \\ W_i^{-} & \text{if } \mathrm{AEC}_i^j < 0 \end{cases} \tag{3.8}$$

the limiting factor on the element/vertex contribution.

The above procedure differs from FCT, as described for finite element schemes in Reference [12], in that it applies separate bounds to each of the cell $\rightarrow$ vertex contributions, providing an extra degree of flexibility for the limiting.

The scheme applies the limiting to the difference between the element contributions of the two underlying schemes. In the case of any explicit fluctuation distribution scheme, the splitting into these components is straightforward, as the vector of nodal residuals $\underline{R}^n$ is assembled directly from the aforementioned element contributions and it is clear from both Equations (2.4) and (2.6) that the component of the vector relating to node i takes the form

$$R_i = \sum_{j \in \cup \triangle_i} \alpha_i^j \phi_j = \sum_{j \in \cup \triangle_i} R_i^j \tag{3.9}$$

a simple sum of neighbouring element contributions. Thus, the fact that

$$\frac{1}{\Delta t}\, \mathbf{M}_{\mathrm{L}} \triangle_n \underline{U}^{\mathrm{L}} = -\underline{R}^n \tag{3.10}$$

in which $\mathbf{M}_{\mathrm{L}}$ is a lumped mass matrix (constructed by analogy with finite element schemes [2,3] and the symbol $\triangle_n(\cdot) = (\cdot)^{n+1} - (\cdot)^n$ represents a time difference, which implies that the element contribution from cell j to node i can be written

$$(\mathrm{L/H})\mathrm{EC}_i^j = \Delta t \mathbf{M}_{\mathrm{L}}^{-1} (\alpha_i^j \phi_j) \underline{1}_i \tag{3.11}$$

in which $\underline{1}_i$ is the vector with zero entries except for the ith component, which takes the value 1. $\mathbf{M}_{\mathrm{L}}$ is simply the diagonal matrix whose non-zero entries are the nodal areas used to weight

the updates in Equations (2.4) or (2.6), so all of the inversion operations are local. The differences between the PSI and the Lax–Wendroff schemes are in the distribution coefficients α_i^j and, if the scheme defined by (2.6) is used, in the definition of the nodal areas that constitute the diagonal entries of $\mathbf{M}_L$. It only remains to choose the values of the limiting coefficients β_k in (3.8).

3.1. The distribution point

Consider a single grid cell in isolation: the distribution point is defined to be the point whose local area co-ordinates are the distribution coefficients of the scheme for that triangle. For simplicity, it will be assumed from now on that the distribution coefficients are non-negative (true for both the Lax–Wendroff and the PSI schemes) so that the distribution point is always within the cell or on its boundary. Figure 1 shows examples of typical distribution points for the two schemes considered here. Note that the distribution point lies on the outflow edge (or at the downstream vertex of a cell with one inflow edge) of the triangle when the scheme is fully upwind.

The relationship between the distribution coefficients and the local area co-ordinates can be written explicitly, using the numbering of Figure 1 and indexing the coefficients by vertex number, as

$$\alpha_1 = \frac{\text{Area } 230}{\text{Area } 123}, \qquad \alpha_2 = \frac{\text{Area } 310}{\text{Area } 123}, \qquad \alpha_3 = \frac{\text{Area } 120}{\text{Area } 123} \tag{3.12}$$

from which it is obvious that

$$\alpha_1 + \alpha_2 + \alpha_3 = 1 \tag{3.13}$$

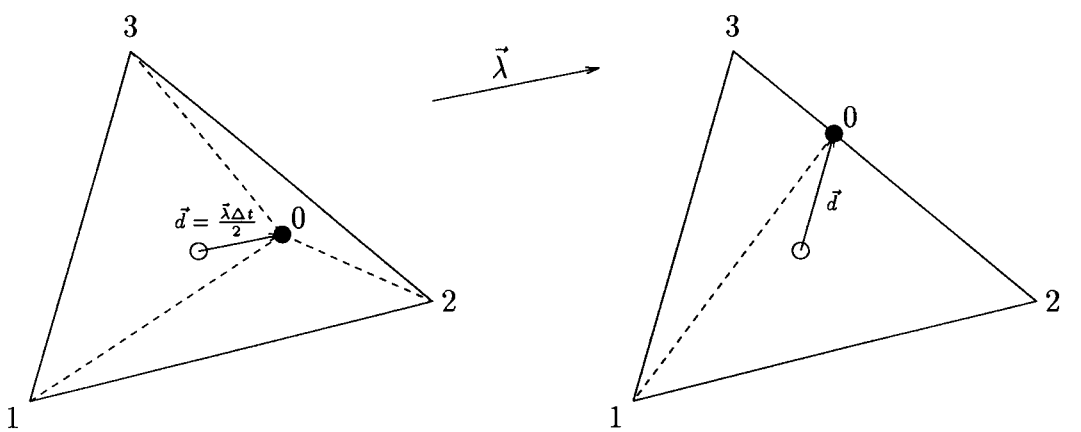

Figure 1. The position of the distribution point for the Lax–Wendroff scheme (left) and in the two-target case for a fully upwind scheme, e.g. PSI (right).

so the scheme is conservative, and that $\alpha_k \geq 0$ as long as the distribution point remains within or on the triangle.

It is useful to note that the movement of the distribution point is equivalent to the redistribution of the fluctuation between the vertices of the triangle. Furthermore, moving the distribution point parallel to an edge keeps constant the proportion of the fluctuation being sent to the opposite vertex, i.e. the redistribution is taking place between the two nodes on that edge.

3.2. The equivalent equation

The diffusion vector $\vec{d}$ labelled in Figure 1 represents the displacement of the distribution point from the centroid of the triangle (the distribution point of a symmetric central scheme). It is useful to note that a scheme with diffusion vector $\vec{d}$ can be shown (see Appendix A) to have the second-order equivalent equation

$$u_t + \vec{\lambda}\cdot\vec{\nabla}u = \vec{d}\cdot\vec{\nabla}(\vec{\lambda}\cdot\vec{\nabla}u) \tag{3.14}$$

The right-hand side of Equation (3.14) represents the numerical diffusion of the distribution scheme and can be used in the analysis of the accuracy of the method.

Further, simple geometric arguments can be used to show that the distribution coefficients of any scheme defined locally by a diffusion vector $\vec{d}_j$ are given by

$$\alpha_i^j = \frac{1}{3} + \frac{1}{2S_{\triangle_j}}\vec{d}_j\cdot\vec{n}_i^j \tag{3.15}$$

The relationship with the Lax–Wendroff scheme is obvious and comparison with (2.14) immediately gives

$$\vec{d}_j = \frac{\vec{\lambda}_j\Delta t}{2} \tag{3.16}$$

as noted in Figure 1.

The equivalent equation can be used to suggest a method of redistributing the fluctuation by first noting that (3.14) may be rewritten

$$u_t + \vec{\lambda}\cdot\vec{\nabla}u = \frac{\vec{\lambda}\Delta t}{2}\cdot\vec{\nabla}(\vec{\lambda}\cdot\vec{\nabla}u) + \left(\vec{d} - \frac{\vec{\lambda}\nabla t}{2}\right)\cdot\vec{\nabla}(\vec{\lambda}\cdot\vec{\nabla}u) \tag{3.17}$$

which introduces the diffusion vector of the Lax–Wendroff scheme (3.16). The first term on the right-hand side of (3.17) represents the numerical diffusion of the Lax–Wendroff scheme, which is second-order accurate, while the second term provides additional, unwanted diffusion. However, any choice of $\vec{d}$ such that

$$\vec{d} - \frac{\bar{\lambda}\Delta t}{2} \perp \vec{\nabla}(\vec{\lambda} \cdot \bar{\nabla} u) \tag{3.18}$$

will make the unwanted term vanish, so the corresponding distribution scheme should be second-order accurate for the given local data. Therefore, moving the distribution point perpendicular to the local value of $\vec{\nabla}(\vec{\lambda} \cdot \vec{\nabla} u)$ should not change of order of accuracy of the local discretization.

It is important to note here that the second derivative in (3.18) can be approximated locally by a first derivative since

$$\vec{\nabla}(\vec{\lambda} \cdot \vec{\nabla} u) = -\vec{\nabla} u_t \tag{3.19}$$

and u_t can be approximated simply from the unlimited high-order update (which has already been calculated as part of this FCT-type limiting procedure) using

$$\vec{\nabla} u_t = \frac{1}{\Delta t} (\vec{\nabla} u^{n+1} - \vec{\nabla} u^n) \tag{3.20}$$

This avoids calculating the second-order spatial derivative that appears in (3.18) directly and allows the overall algorithm to remain compact, as Equation (3.20) still involves only local operations.

3.3. The monotonicity region

The bounds defined by Equation (3.8) can be used to construct a region within each triangle, inside which all distribution points guarantee a monotone scheme. An example of such a monotonicity region is shown shaded in Figure 2.

The monotone scheme is constructed from low-order (LO) and high-order (HO) updates. When combined like this is it considerably simpler to use the form (2.4) for the nodal updates of both schemes, so the limited distribution coefficients can be expressed as

$$\alpha_i^j = (\alpha_i^j)^{\mathrm{LO}} + \beta_i^j((\alpha_i^j)^{\mathrm{HO}} - (\alpha_i^j)^{\mathrm{LO}}) \tag{3.21}$$

in which the β_i^j are precisely the limiting coefficients of (3.8). The more accurate low-order update (2.6) would require the coefficients in Equation (3.21) to be scaled by the weighted nodal areas. From (3.21) it can be seen that $\beta_i^j = 0$ leads to the PSI coefficients, while $\beta_i^j = 1$ returns the Lax–Wendroff scheme.

Conservation requires that

$$\sum_{i \in \triangle_j} \alpha_i^j = 1, \quad \forall j \tag{3.22}$$

so

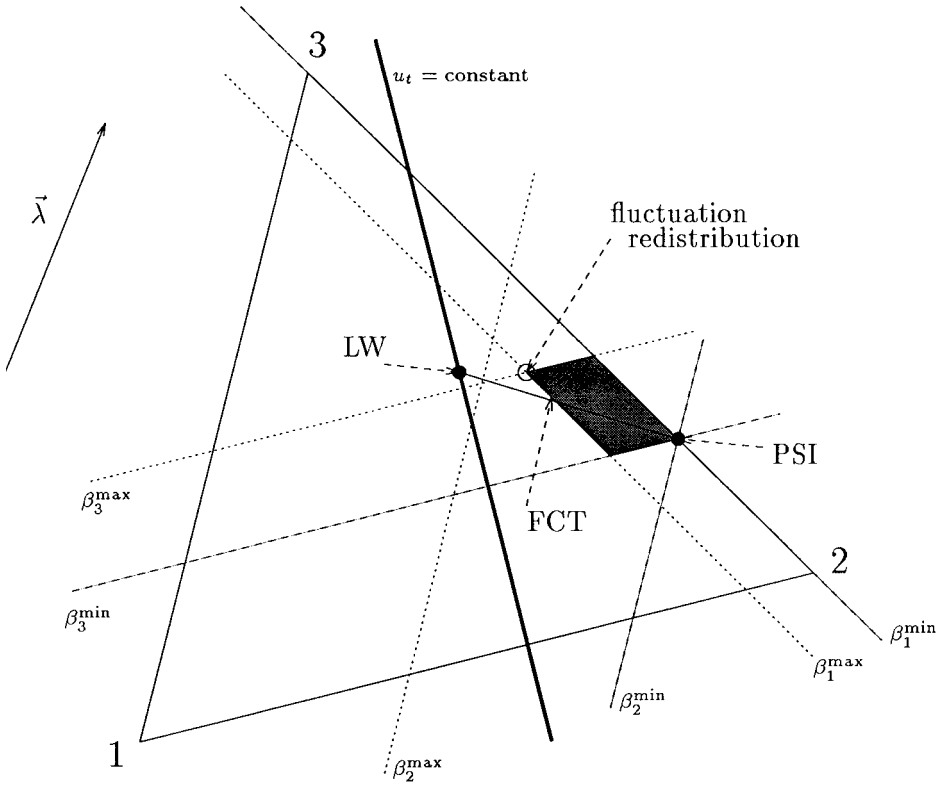

Figure 2. A monotonicity region (shaded dark grey) for the distribution point based on the PSI and Lax–Wendroff schemes.

$$\sum_{i\in\triangle_j} \beta_i^j((\alpha_i^j)^{\mathrm{HO}} - (\alpha_i^j)^{\mathrm{LO}}) = 0 \tag{3.23}$$

There are three terms in the sum on the left-hand side of (3.23), which represent, depending on one's point of view, either the displacement of the distribution point from that of the PSI scheme (in terms of area co-ordinates) or the additional contributions from the fluctuation to the corresponding vertices of the cell.

In general

$$(0 =)\ (\beta_i^j)^{\min} \le \beta_i^j \le (\beta_i^j)^{\max}\ (\le 1) \tag{3.24}$$

which describes a pair of 'tramlines' parallel to edge i of triangle j, and illustrated in Figure 2 for a single triangular cell by dashed/dotted lines. The bounds $0 \le \beta_i^j \le 1$ have been imposed here for simplicity. They can, with some effort, be extended considerably [7] but we do not yet have convincing motivation to recommend this. As it stands, the monotonicity region (shaded

grey in the figure) lies within the triangle and between the distribution points of the two underlying schemes. Placing the distribution point anywhere within this shaded area ensures that the subsequent nodal updates will not create any new local extrema at the next time level and, as a result, imposes stability on the scheme. In order to maintain accuracy, the distribution point can be positioned optimally by placing it at the point within the monotonicity region that lies closest to the contour line of u_t passing through the high-order distribution point, minimizing the additional numerical diffusion in the related equivalent equation (3.17).

Note that the perpendicular distance of each tramline from its parallel cell edge depends linearly on the corresponding β and that $\beta = 0$ defines a line passing through the low-order distribution point, while $\beta = 1$ corresponds to the parallel line through the high-order distribution point. The linear dependence allows the monotonicity region to be constructed from simple geometric considerations. Furthermore, it implies that FCT, which for cell j is given by

$$\beta_i^j = \min_{i \in \triangle_j} (\beta_i^j)^{\max}, \quad \forall i \in \triangle_j \tag{3.25}$$

will position the distribution point at the intersection of the straight line joining the Lax–Wendroff and the PSI distribution points with the boundary of the monotonicity region, as shown in Figure 2.

3.4. Fluctuation redistribution

Two schemes have been described in Section 2, one having second-order accuracy (Lax–Wendroff) and the other being monotonic (PSI), which can be combined to produce a new scheme with improved properties. In essence, this procedure involves constructing the monotonicity region of Section 3.3, finding the distribution point within this region that minimizes the error term according to the equivalent equation (3.17), and finally redistributing the fluctuation accordingly. The position to which the distribution point is moved depends not only on the extent of the monotonicity region but also on the 'preferred direction' (perpendicular to a local approximation of $\vec{\nabla} u_t$) suggested by the equivalent equation (3.17).

The calculation of the limited distribution coefficients therefore takes the following form:

- Construct the monotonicity region surrounding the low-order distribution point using the bounds on the cell $\rightarrow$ vertex contributions defined by (3.8).
- Find the line passing through the high-order distribution point perpendicular to the locally constructed value of $\vec{\nabla} u_t$ (i.e. a contour line of u_t).
- Calculate the position of the point in the monotonicity region closest to the line defined above and take this to be the distribution point of the limited scheme. If the line intersects the region then take the point of intersection closest to the high-order distribution point. (Note that when the contour line does not intersect the monotonicity region, the limited distribution point will be at a corner of the region.)

The limited distribution point for the example illustrated in Figure 2 is indicated by a circle.

4. RESULTS

The practical order of accuracy of the new scheme has been investigated using various test problems, the first of which is the advection of an initial profile given by the double sine wave function

$$u = \sin(2\pi x)\sin(2\pi y) \tag{4.1}$$

with velocity $\vec{\lambda} = (1, 2)^T$ over the domain $[0, 1] \times [0, 1]$. Periodic boundary conditions are applied and the solutions are compared at $t = 1.0$ when they should have returned to the initial profile. $\Delta t/\Delta x = 0.32$ for each computation, giving a Courant–Friedrich–Lewy (CFL) number of about 0.716, unless stated otherwise.

We compare the present scheme with various alternative methods and make the comparison on two different types of grid, shown in Figure 3. Each is simply a square grid with diagonals added either consistently (type A) or in an alternating fashion (type B). In type A grids all interior nodes belong to six elements, but in type B grids they may belong to either four or eight. Some schemes are sensitive to this difference and can be expected to perform less well if the grid is completely unstructured.

Solution profiles obtained on the two 32×32 grids shown in Figure 3 are illustrated in Figures 4 and 5, along with the exact solution. The PSI scheme (with upwind weighted nodal areas, as in Equation (2.6)) is clearly the most diffusive of those shown, most markedly in the streamwise direction, which, together with the non-alignment of the flow with the mesh edges, causes some distortion of the profile. There are only minor differences between the solutions obtained using the Lax–Wendroff and fluctuation redistribution schemes and apart from a small phase lag, typical of Lax–Wendroff type schemes, both retain the shape of the exact

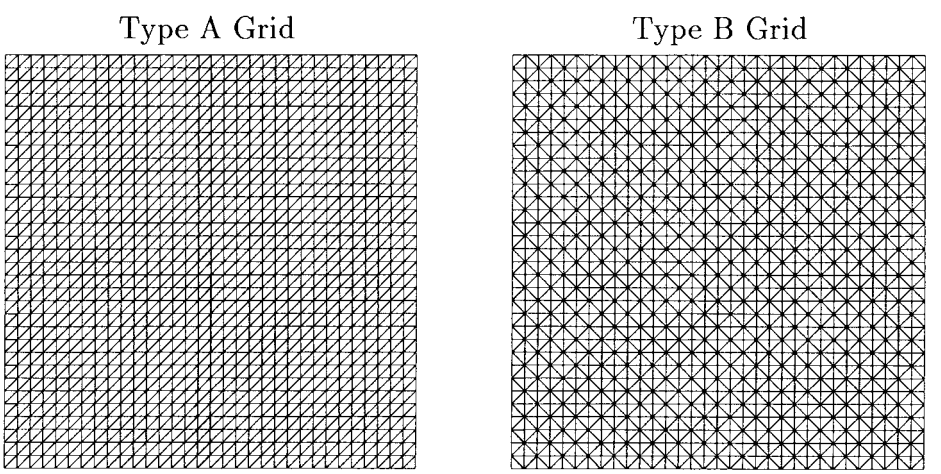

Figure 3. The two types of grid used.

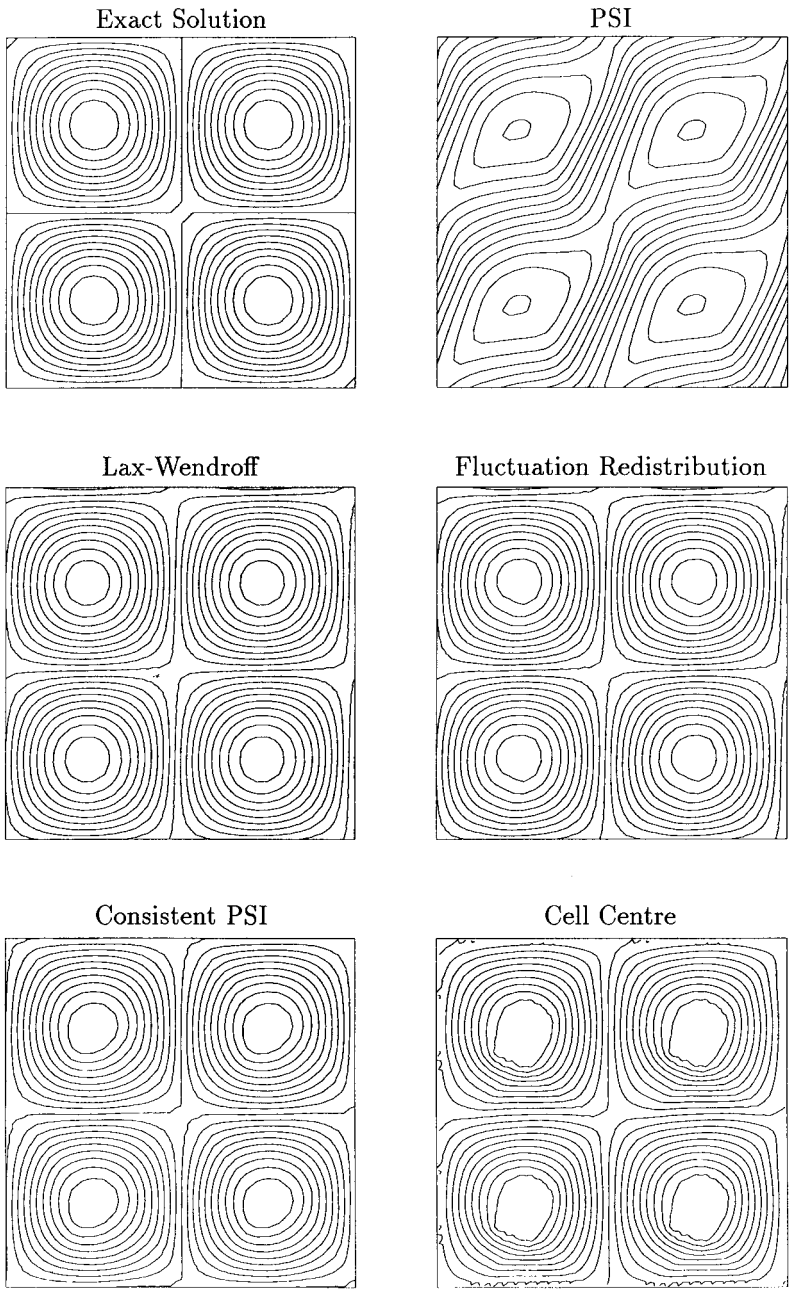

Figure 4. Solutions for the double sine wave test case on grid A.

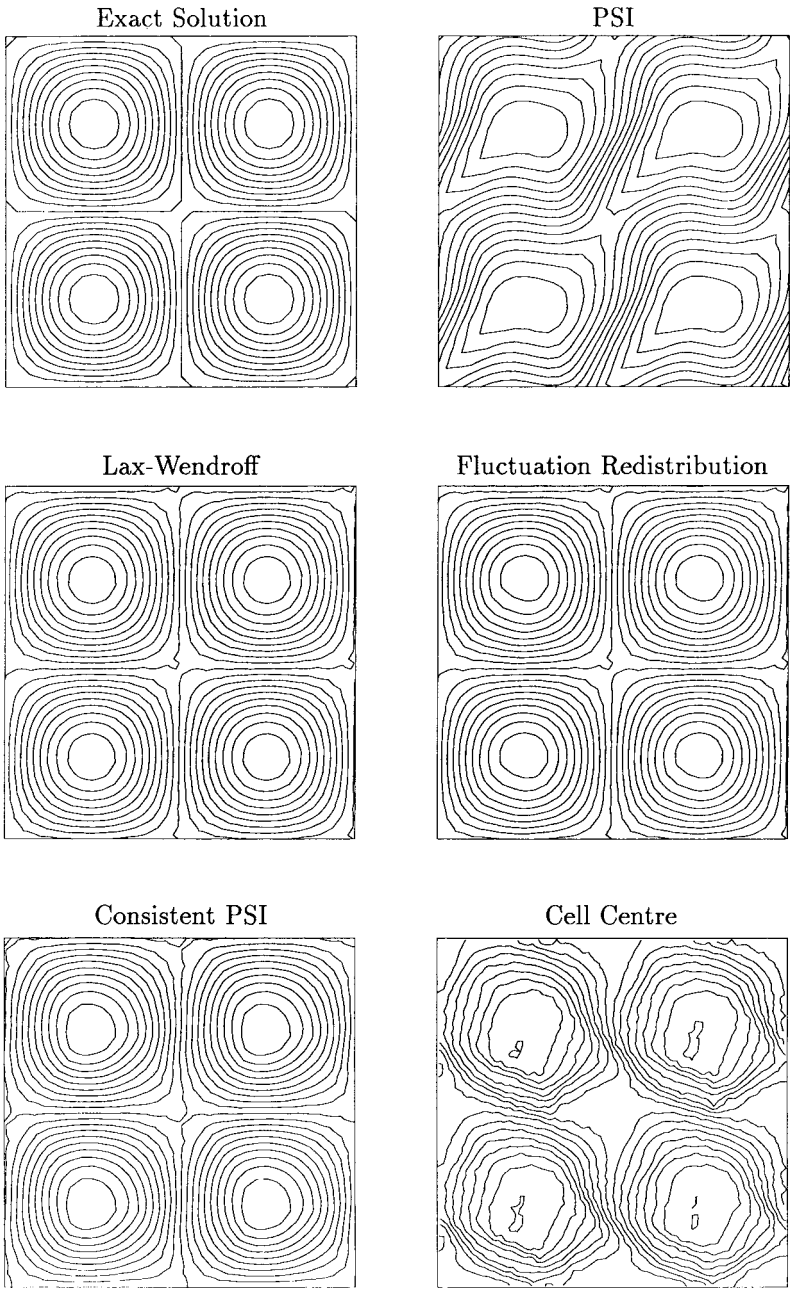

Figure 5. Solutions for the double sine wave test case on grid B.

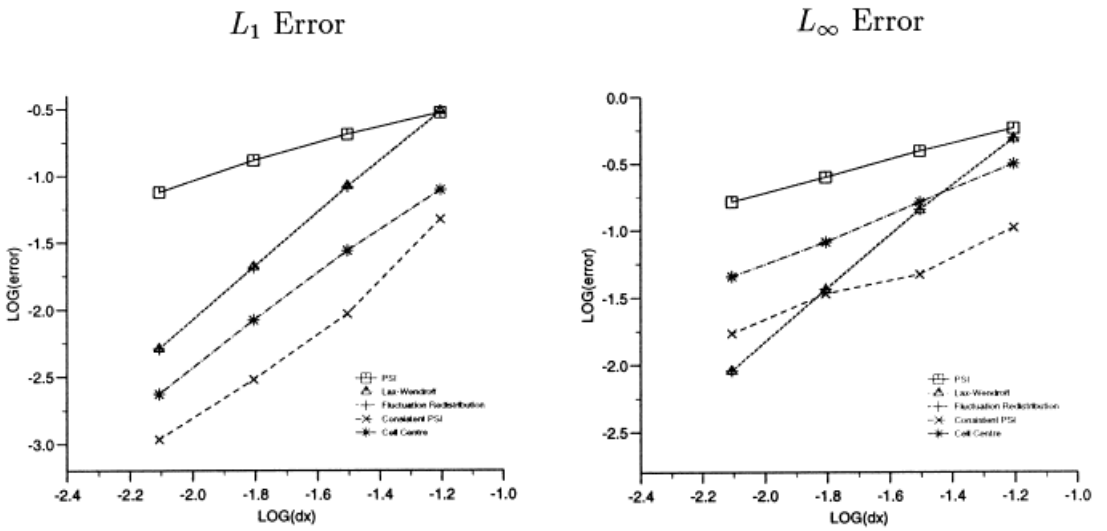

Figure 6. Errors for the double sine wave test case on grid A.

solution. The consistent PSI scheme presented is that of März [3] with Crank–Nicolson implicit time stepping combined with the standard explicit PSI scheme via FCT to enforce monotonicity [2]. This solution has been calculated using half the time step of the others since there is a significant loss of accuracy and distortion of the solution profile when the higher CFL number is used. The cell centre upwind scheme (the maximum limited gradient (MLG) scheme of Reference [16]) used to produce the final solution, is also run at half the time step, this time because the scheme becomes unstable otherwise. Furthermore, of all the schemes tested, the cell centre scheme shows the greatest dependence on the orientation of the grid cells, giving a considerably worse solution on the type B grid.

The effectiveness of the new method is illustrated further in Figures 6 and 7. (All results have been obtained on grids of the same structure as that shown in Figure 3.) Most notably, the errors for the fluctuation redistribution are almost indistinguishable from those of the unlimited Lax–Wendroff scheme on each of the grids and the figures in Table I show that both schemes achieve second-order accuracy. This has been the case on all regular grids tested.

The PSI scheme is, unsurprisingly, the least accurate (the upwind weighted updates (2.6) used here being slightly better than the standard approach). Less expected is the poor performance of the cell centre upwind scheme (the MLG scheme of Reference [16]) used here for comparison, which, although second-order in terms of the L_1 error on grid A, reduces to at best first-order in each of the other cases. The consistent PSI scheme also performs poorly on type B grids, particularly as the mesh is refined when the error can even increase. When the diagonal grid edges are all aligned with the flow direction, third-order accuracy can be achieved, repeating the improvement shown when a consistent mass matrix is included in the one-dimensional scheme, but the order of accuracy seen here is at most two. It should also be

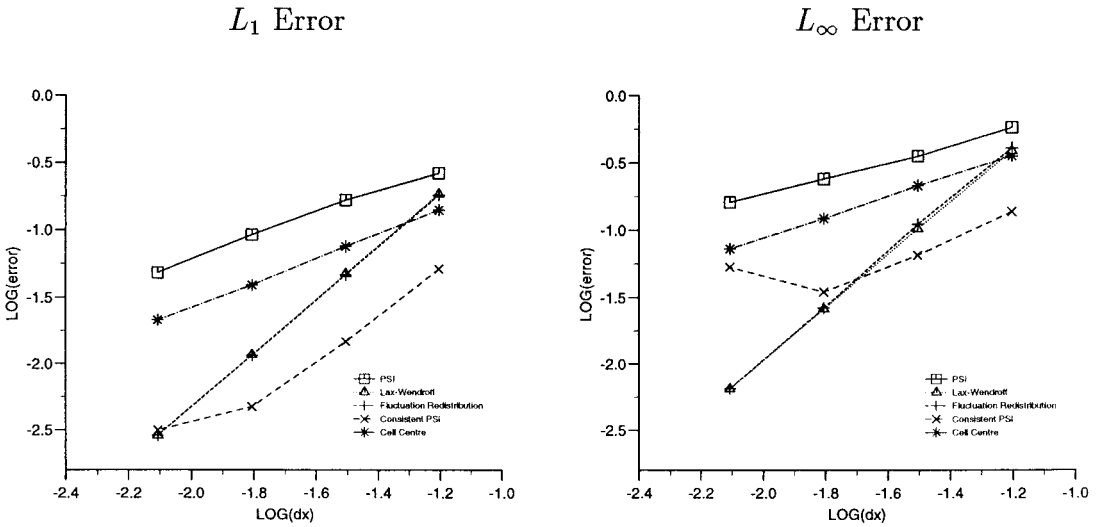

Figure 7. Errors for the double sine wave test case on grid B.

Table I. Numerical orders of accuracy for the double sine wave test case and peak solution values for the rotating cone test case.

Scheme	Grid type A			Grid type B		
	L_1	L_∞	Peak	L_1	L_∞	Peak
PSI	0.79	0.61	0.33	0.93	0.58	0.35
Lax–Wendroff	2.01	2.00	0.81	2.02	2.00	0.82
Fluctuation redistribution	2.00	2.01	0.76	2.01	2.02	0.76
Consistent PSI	1.48	0.98	0.86	0.58	—	0.91
Cell centre	1.82	0.85	0.93	0.87	0.75	0.62

noted that the inversion of the full mass matrix required for this scheme and the smaller time step used make it considerably more expensive than the fluctuation redistribution scheme. Note though, that the extra expense of the matrix inversion is of little consequence in other types of problem, e.g. advection–diffusion, where implicit time stepping will be used so there is no additional cost induced by using a consistent mass matrix.

In the above comparisons, the FCT approach could be applied to the fluctuation distribution scheme instead of the more general redistribution used here. In most of the experiments carried out, the two solutions are almost indistinguishable, e.g. when the limiter is rarely applied, although it is noticeable that the fluctuation redistribution improves relative to FCT as the mesh is refined. However, there are occasions when the extra flexibility of the fluctuation redistribution scheme provides a dramatic improvement in the quality of the

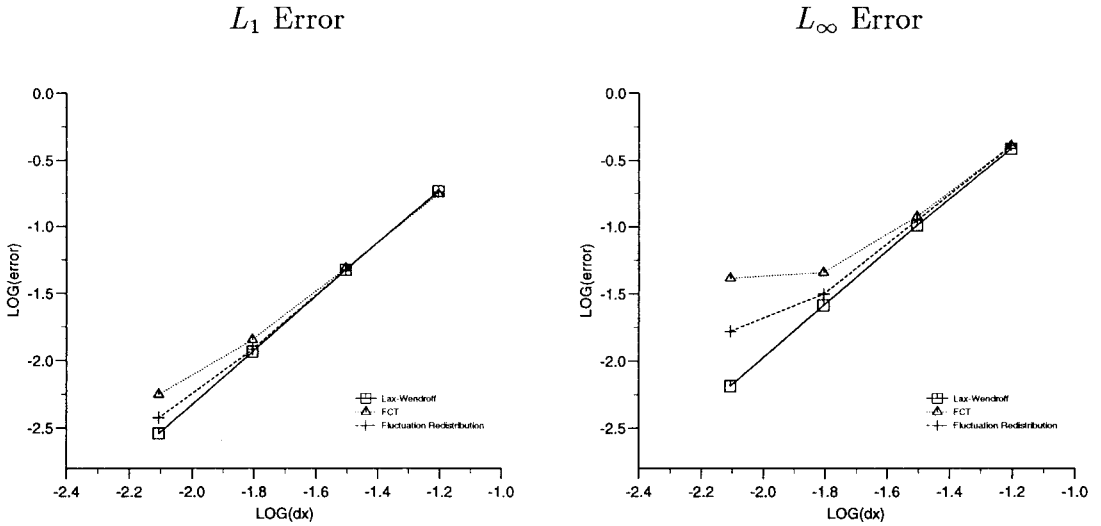

Figure 8. Errors for the double sine wave test case on grid B.

solution. Figure 8 shows the solution accuracy on type B grids for both schemes when the monotonicity region, as described in Section 3.3, is restricted (by removing the dependence on u^{L} in the first computation of (3.5), and illustrates the advantage of the more flexible approach, particularly as the grid gets finer.

The second test case presented here involves the circular advection of the 'cone' given by the initial conditions

$$u = \begin{cases} \cos^2(2\pi r) & \text{for } r \leq 0.25 \\ 0 & \text{otherwise} \end{cases} \tag{4.2}$$

where $r^2 = (x + 0.5)^2 + y^2$, with velocity $\vec{\lambda} = (-2\pi y,\ 2\pi x)^T$ around the domain $[-1, 1] \times [-1, 1]$, the solution being continually set to zero at each of the inflow boundaries. The initial profile should be advected in a circle without change of shape until it returns to its original position when $t = 1.0$. In the numerical experiments the ratio $\Delta t/\Delta x = 0.08$, giving a maximum CFL number of approximately 0.711.

Solution profiles obtained on a 64×64 type A grid are presented in Figure 9. (The solutions obtained on the type B grid are very similar except for the cell centre scheme, which is considerably more diffusive, as indicated by the peak solution values shown in Table I.) The PSI scheme is again clearly the most diffusive (most markedly in the streamwise direction). This is confirmed by the peak values in Table I. Note that the standard PSI scheme (using (2.4) rather than (2.6)) gives a peak value of only 0.22 after one revolution. The Lax–Wendroff scheme keeps the height of the peak much better but oscillations are obvious in the wake of

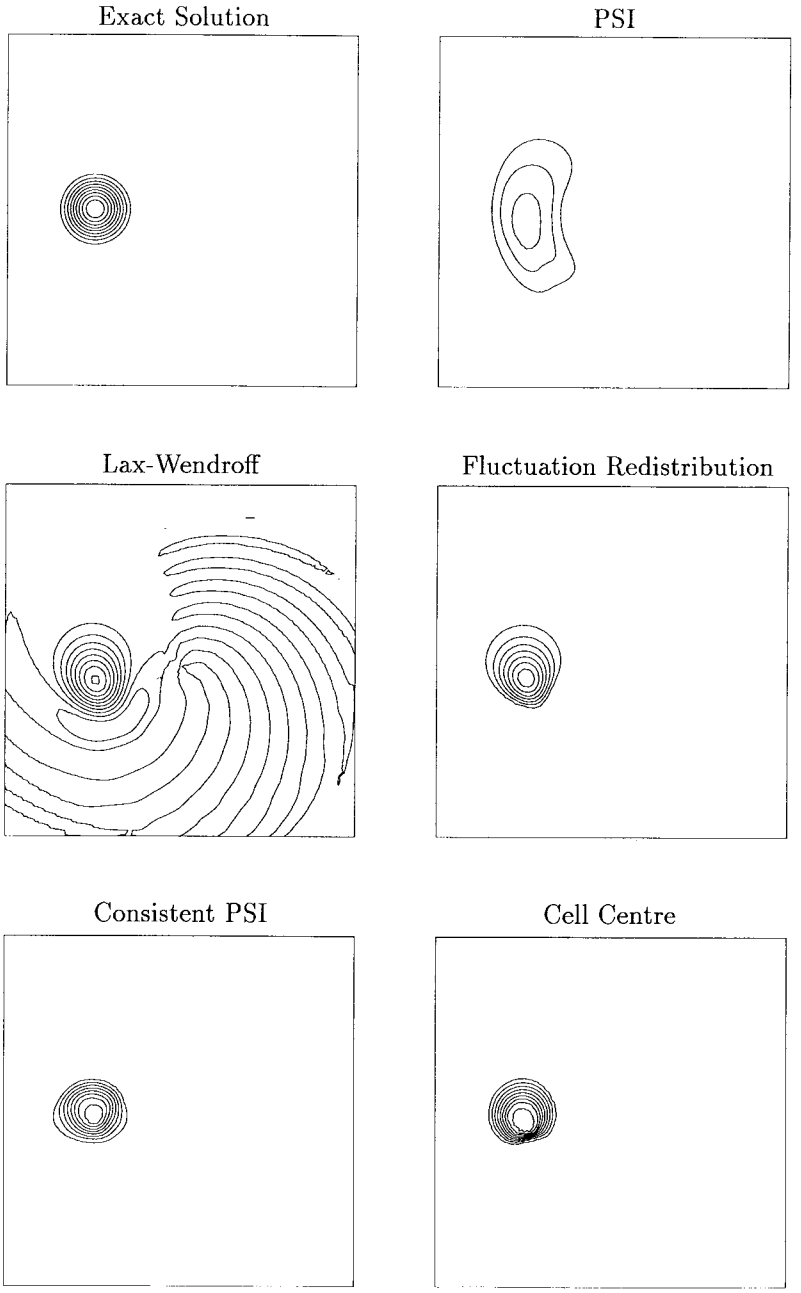

Figure 9. Solutions for the rotating cone test case on grid type A.

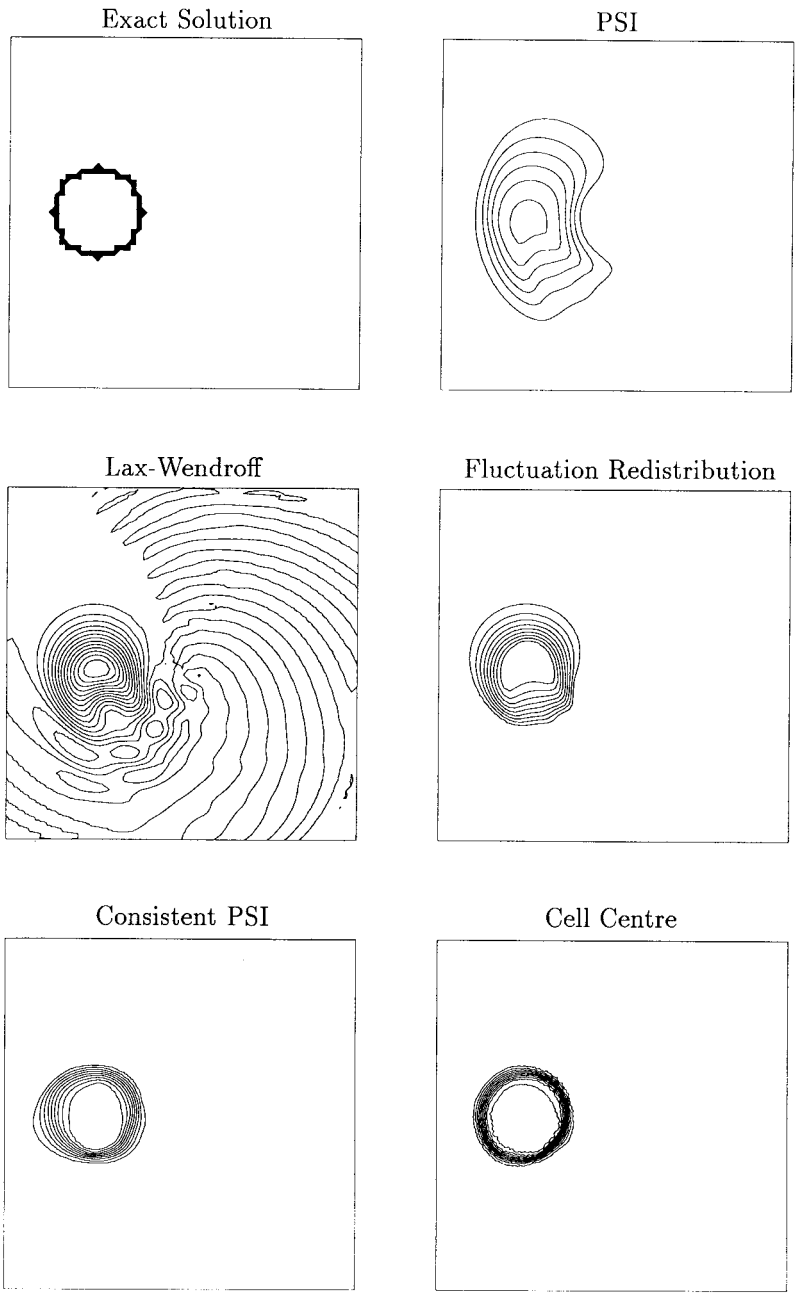

Figure 10. Solutions for the rotating cylinder test case on grid type A.

the cone—and less clearly there is a small phase lag, which positions the peak slightly upstream of its correct position. The fluctuation redistribution scheme retains the accuracy of the Lax–Wendroff scheme without any unwanted oscillations, but still shows the phase lag of the parent method. The consistent PSI scheme is clearly the best of the cell vertex schemes compared since it not only retains the peak but has negligible phase lag. The cell centre scheme gives a comparable solution on this grid, but suffers badly on type B grids.

Finally, a similar but discontinuous test case is presented. The domain, velocity, boundary conditions and CFL number remain unchanged, but the new initial solution profile is a cylinder, given by

$$u = \begin{cases} 1 & \text{for } r \leq 0.25 \\ 0 & \text{otherwise} \end{cases} \tag{4.3}$$

where $r = (x + 0.5)^2 + y^2$. Qualitatively, the solutions shown in Figure 10 exhibit the same properties as the corresponding rotating cones, although in this case the cell centre scheme gives clearly the best solution (on the type B grid it deteriorates considerably and only the solution obtained from the PSI scheme is more diffusive).

It is clear from the solutions presented that the fluctuation redistribution scheme is genuinely second-order accurate on regular grids. The other monotonic schemes with which it has been compared will sometimes produce better solutions, but this is usually on very regular grids and when the flow direction is aligned with grid edges. In more general situations, the other schemes fare considerably worse, e.g. on a simple regular grid in which the diagonals alternate in direction, while the fluctuation redistribution maintains its accuracy, almost independently of the grid.

5. CONCLUSIONS

In this paper the problem of achieving high-order accurate numerical solutions to the two-dimensional scalar advection equation on triangular grids using upwind fluctuation distributions schemes has been addressed.

An approach similar to FCT in philosophy, but having greater flexibility, has been described, which puts together a low-order monotone scheme with a high-order scheme to combine the properties of the two. The procedure involves a redistribution of the fluctuation to impose monotonicity. Bounds on nodal contributions are calculated in a manner similar to FCT and the distribution coefficients are then altered so that these bounds are satisfied. Analysis of the equivalent equation of the scheme reveals that there is also a preferred direction for the movement of the distribution point—a point that geometrically represents the fluctuation distribution within a cell, which allows second-order accuracy to be attained more extensively by the limited scheme. FCT is a special case of fluctuation redistribution.

In practice, combining the PSI and the Lax–Wendroff schemes via fluctuation redistribution has achieved second-order accuracy on simple test problems; in particular, it shows little loss of accuracy near smooth extrema. It has been compared with a consistent upwind finite

element scheme [3], also developed to enhance the properties of multi-dimensional upwind schemes for time-dependent flows. It is considerably less expensive than the consistent PSI scheme, and although not as accurate on grids with regular connectivity (type A), it is often more accurate on grids with irregular connectivity (type B). It is also consistently more accurate than any of the high resolution, triangle-based, cell centre finite volume schemes presented in Reference [16].

All of the techniques here generalize to three-dimensional advection straightforwardly. They also apply to the advective components of multi-dimensional systems of equations [4,17], and inhomogeneous equations can be dealt with either by including the source terms within the decomposition and distributing them as such or by treating the source terms separately, using an implicit discretization where necessary. The remaining questions to be answered for application to three-dimensional or unsteady systems have to do with the analytical nature of the decompositions.

ACKNOWLEDGMENTS

The authors would like to thank Professor M.J. Baines for his contributions to this work and the EPSRC for providing the funding for the first author under grant number GR/K74616.

APPENDIX A. DERIVATION OF THE EQUIVALENT EQUATION

The object of this appendix is to establish the relationship between the equivalent equation of an advection scheme of fluctuation splitting type and the location of the distribution point. Recall that the equivalent equation is the differential equation which a numerical scheme actually solves, rather than the one which it purports to solve. Usually, the equivalent equation is of infinite order, corresponding to the infinite Taylor expansion of the truncation error, but in practice only the leading terms convey useful information.

In the present context, we reverse the usual analysis by specifying the equivalent equation. In fact we pretend that we actually wish to solve the problem defined by

$$u_t + \vec{\lambda}\cdot\vec{\nabla}u = \vec{d}\cdot\vec{\nabla}(\vec{\lambda}\cdot\vec{\nabla}u) \tag{A.1}$$

and that we wish to solve it by a first-order method. Here, $\vec{d}$ is an arbitrary vector defining a diffusive right-hand side of a particular form. This diffusion vanishes in the steady state. For the equation to be dimensionally correct, $\vec{d}$ must have the dimensions of a length, and we will take it to be a constant.

Now we will update the node i by integrating (A.1) over the area S_i of the dual cell associated with node i

$$S_i \frac{\partial u_i}{\partial t} = -\iint_{S_i} \vec{\lambda}\cdot\vec{\nabla}u \,\mathrm{d}x\,\mathrm{d}y + \iint_{S_i} \vec{d}\cdot\vec{\nabla}(\vec{\lambda}\cdot\vec{\nabla})\,\mathrm{d}x\,\mathrm{d}y \tag{A.2}$$

Using Gauss' theorem and the assumption that $\vec{d}$ is constant, this becomes

$$S_i \frac{\partial u_i}{\partial t} = -\iint_{S_i} \vec{\lambda}\cdot\vec{\nabla}u \, \mathrm{d}x \, \mathrm{d}y + \oint_{\partial S_i} (\vec{\lambda}\cdot\vec{\nabla}u)\vec{d}\cdot\mathrm{d}\vec{n} \tag{A.3}$$

where $\vec{n}$ is the outward normal to the boundary ∂S_i of the cell.

Since u is supposed linear within each triangle, the integrands are piecewise constant. Also, the triangle $\triangle_j$, whose vertices are i, j, $j+1$ (see Figure A1) makes a contribution to the line integral proportional to

$$\int_{\triangle_j} \mathrm{d}\vec{n} = \frac{1}{2}(\vec{r}_{j+1} - \vec{r}_j) \times \vec{i}_z \tag{A.4}$$

where $\vec{i}_z$ is a unit vector pointing out of the paper and $\vec{r}_j$ is the position of vertex j in the x–y plane. So the time derivative of u_i can be rewritten

$$\begin{aligned} S_i \frac{\partial u_i}{\partial t} &= \sum_{j \in \cup \triangle_i} S_{i\cap j} \frac{\phi_j}{S_j} - \sum_{j \in \cup \triangle_i} \frac{\phi_j}{S_{\triangle_j}} \left(\frac{1}{2} \vec{d}\cdot(\vec{r}_{j+1} - \vec{r}_j) \times \vec{i}_z \right) \\ &= \sum_{j \in \cup \triangle_i} \frac{\phi_j}{S_{\triangle_j}} \left[S_{i\cap j} - \frac{1}{2} \vec{d}\cdot(\vec{r}_{j+1} - \vec{r}_j) \times \vec{i}_z \right] \end{aligned} \tag{A.5}$$

Here $S_{\triangle_j}$ is the area of $\triangle_j$ and $S_{i\cap j}$ is the area common to S_i and $\triangle_j$; if we choose the dual cells, geometrically it is $S_j/3$.

Now let $\vec{C}_j$ be the position vector of the centroid of $\triangle_j$ and let $\vec{D}_j = \vec{C}_j + \vec{d}$. The triple product, with the factor 1/2 can be identified with the area S_{ACBDA} so that

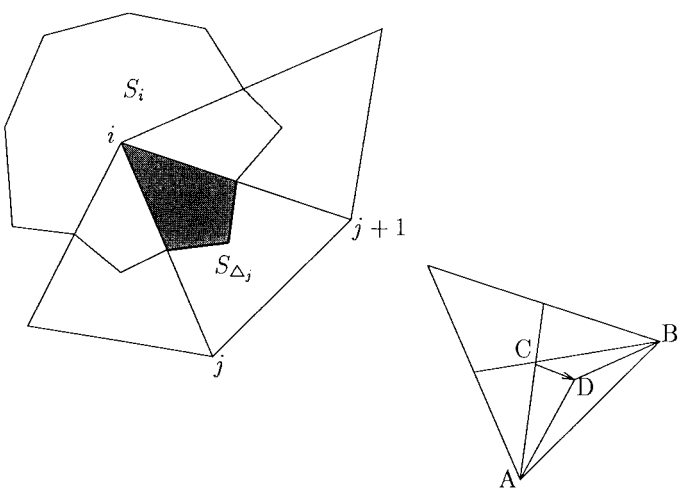

Figure A1. Geometry of grid. The triangle $\triangle_j$ with vertices i, j, $j+1$ is redrawn in isolation. The diffusion vector is $\vec{d} = \overrightarrow{CD}$.

$$\frac{1}{2}\vec{d}\cdot(\vec{r}_{j+1}-\vec{r}_j)\times\vec{i}_z = S_{\mathrm{ACB}} - S_{\mathrm{ADB}} = \frac{1}{3}S_j - S_{\mathrm{ADB}} \tag{A.6}$$

Hence

$$S_i\frac{\partial u_i}{\partial t} = \sum_{j\in\cup\triangle_i}\frac{\phi_j}{S_j}\left[\frac{1}{3}S_j - \left(\frac{1}{3}S_j - S_{\mathrm{ADB}}\right)\right] = \sum_{j\in\cup\triangle_i}\phi_j\frac{S_{\mathrm{ADB}}}{S_j} = \sum_{j\in\cup\triangle_i}\phi_j\bar{S}_i(\vec{D}_j) \tag{A.7}$$

where $\vec{D}_j$ is the distribution point in $\triangle_j$ and $\bar{S}_i(\vec{D}_j)$ is its area co-ordinate in that triangle with respect to vertex i.

Conversely, we can say that if the distribution point is chosen in this manner, then (A.1) is the equivalent equation.

To create a scheme that is second-order in time we solve by this first-order method the equivalent equation

$$u_t + \vec{\lambda}\cdot\vec{\nabla}u = \frac{\Delta t}{2}\vec{\lambda}\cdot\vec{\nabla}(\vec{\lambda}\cdot\vec{\nabla}u) \tag{A.8}$$

where the term on the right is the second-order correction $(\Delta t/2)u_{tt}$ for the original advection problem. Therefore, we take $\vec{d} = \vec{\lambda}\Delta t/2$, which gives the Lax–Wendroff version of fluctuation splitting, and the unique member of the family that is second-order in time. To obtain steady states that are second-order accurate $\vec{d}$ should be chosen parallel to $\vec{\lambda}$. This analysis is valid provided that $\vec{d}$ is either constant or else varies more slowly than the solution.

REFERENCES

1. Deconinck H, Struijs R, Bourgois G, Roe PL. High resolution shock capturing cell vertex advection schemes for unstructured grids. In *Computational Fluid Dynamics*. Number 1994-05 in von Karman Institute Lecture Series, 1994.
2. Hubbard ME, Roe PL. Multidimensional upwind fluctuation distribution schemes for scalar time dependent problems. Numerical Analysis Report 1/98, Department of Mathematics, University of Reading, 1998.
3. März J. *Improving Time Accuracy for Residual Distribution Schemes*. VKI PR-1996-17, von Karman Institute for Fluid Dynamics, 1996.
4. Paillère H, van der Weide E, Deconinck H. Multidimensional upwind methods for inviscid and viscous compressible flows. In *Computational Fluid Dynamics*. Number 1995-12 in von Karman Institute Lecture Series, 1995.
5. Sidilkover D, Roe PL. Unification of some advection schemes in two dimensions. ICASE Report 95-10, 1995.
6. Struijs R. A multi-dimensional upwind discretization method for the Euler equations on unstructured grids. PhD Thesis, The University of Delft, The Netherlands, 1994.
7. Struijs R. The fluctuation splitting method. In *Numerical Methods for Advection–Diffusion Problems*, Vreugendhill CB, Koren B (eds). Vieweg: Wiesbaden, 1993.
8. Deconinck H, Koren B. *Euler and Navier–Stokes Solvers using Multidimensional Upwind Schemes and Multigrid Acceleration. Results of the BRITE/EURAM Projects 1989–1995*. Vieweg: Wiesbaden, 1997.
9. Roe PL, Mesaros LM. Solving steady mixed conservation laws by elliptic/hyperbolic splitting. In *Fifteenth International Conference on Numerical Methods in Fluid Dynamics*. Monterey, Kutler P, Flores J, Chattot J-J (eds). 1996.
10. Khobalatte B, Leyland P. New finite element based fluctuation splitting kinematic schemes. *International Journal for Numerical Methods in Fluids* 1998; **27**: 229–239.
11. Ferrante A. *Solution of the Unsteady Euler Equations using Residual Distribution and Flux Corrected Transport*. VKI PR 1997-08, von Karman Institute for Fluid Dynamics, 1997.

12. Löhner R, Morgan K, Vahdati M, Boris JP, Book DL. FEM–FCT: combining unstructured grids with high resolution. *Communications in Applied Numerical Methods* 1988; **4**: 717–729.
13. MacCormack RW. The effect of viscosity in hypervelocity impact cratering. AIAA Paper 69-354, 1969.
14. van Leer B. Towards the ultimate conservative difference scheme V. A second order sequel to Godunov's method. *Journal of Computational Physics* 1979; **32**: 101–136.
15. Zalesak ST. Fully multi-dimensional flux-corrected transport algorithms for fluids. *Journal of Computational Physics* 1979; **31**: 335–362.
16. Batten P, Lambert C, Causon DM. Positively conservative high-resolution convection schemes for unstructured elements. *International Journal for Numerical Methods in Engineering* 1996; **39**: 1821–1838.
17. Mesaros LM, Roe PL. Multidimensional fluctuation-splitting methods based on decomposition methods. AIAA 95-1699 CFD Conference AIAA CP-956, 1995.

